Structural, electronic and optical properties of the Half-Heusler MgYGa alloy Via DFT calculations

H. Kamel[a], G. Youcef[a], B. Nabil[b], B. Samir[b], M. Ahmed[a] and C. Abdelali[c],

[a]*Thin-film physics and advanced technologies laboratory, University of Relizane, Algeria.*
[b]*Laboratory of Micro and Nanophysics, National Polytechnic School Oran, ENPO-MA, BP 1523, El M'Naouer, 31000, Oran, Algeria.*
[c]*University of Relizane, Algeria.*

Received 29 September 2023; accepted 20 February 2024

Ab initio calculation of the structural, electronic and optical properties of half-Heusler MgYGa alloy are reported using the FP-LAPW approach of the Density Functional Theory. Generalized Gradient Approximation was used as the exchange and correlation potential for investigating these properties. Structural properties of MgYGa alloy, such as the lattice constants, bulk modulus and pressure derivative of the bulk module have been studied. Electronic properties were investigated by calculating and analyzing the electronic band structure, partial and total density of states graphs for the MgYGa compound. We have found that MgYGa compound has a metallic character. The investigation of optical properties indicates a great interaction between the compound and the incident light.

Keywords: MgYGa alloy; structural properties; optical properties; density functional.

DOI: https://doi.org/10.31349/RevMexFis.70.030502

1. Introduction

Half-Heusler (HH) materials are considered novel materials for energy technology and are potential thermoelectric materials due to their high temperature stability [1-3]. These compounds have attracted considerable interest both theoretically and experimentally due to their ambitious physical properties that allow them to be used for spintronic [4], thermodynamic [5], thermoelectric [6], tunnel junctions or GMR devices [7-10] and optoelectronic applications [11]. The half-Heusler XYZ alloys can be considered as compounds composed of two parts, a covalent part and an ionic part. The X and Y atoms have a distinct cationic character, while Z can be considered as the anionic equivalent [12,13]. Due to the progress in spintronics, half- Heusler compounds have been the subject of numerous studies, motivated by their importance in this field of application [14-16]. The HH alloys comprise a new class of semiconductors [7] highly recommended for use in thermoelectric applications [17-19]. On the other hand, half metallic ferromagnets (HMF's) are a new class of materials with very interesting physical properties. This class of materials presents a conductive nature for one spin channel and a semiconducting nature for the other. These materials are therefore able to generate a fully spinbiased current and thus optimize the efficiency of the spintronic device. Theoretically, four types of HMF's have been predicted: perovskites, zinc blend compounds, oxides and Heusler alloys [20]. De Groot *et al.*, were the first to predict the half-metallicity in a half-Heusler material with the compound MnNiSb [21]. After this prediction a considerable scientific study has been accomplished by the diversified study of HMF's half- Heusler alloys in both theoretical [22-26] and experimental fields [27-29]. The half-Heusler XYZ alloys crystalize in a non-centrosymmetric cubic structure (space group F43m, n$^\circ$ 216) known as structure C_{1b} [30]. This structure is characterized by the interpenetration of three face-centered cubic (cfc) sublattices with atomic sites 4a (0,0,0), 4b (1/2,1/2,1/2) and 4c (1/4,1/4,1/4). In principle, three non-equivalent atomic arrangements are possible in this type of structure [31].

The main objective of this work is to contribute to the study of the structural, electronic and optical properties of MgYGa compound. We have organized our work as follows: In the first part, we have presented an introduction which gives general information on half-Heusler alloys and their applications. The second part contained a brief review of the computational techniques used in this study. The third part is dedicated to the presentation and discussion of the results obtained. Finally, we have concluded with a general conclusion that regroups all the main results of this work.

2. Computational details

The computations in this study have been performed by the full-potential linearized augmented plane wave (FP-LAPW) approach [32] based on the density theory framework (DFT) [33] as implemented in the Wien2k code [34]. The potential exchange and correlation had been treated by the generalized gradient approximation (GGA) parameterized by Perdew-Burke-Ernzerhof (PBE - GGA) [35]. It is well known that the approximation (GGA) underestimates the energy gaps. For this, we used the new approximation developed by Tran and Blaha [36] noted (TBmBJ) (modified Becke-Johnson). This functional is a modern version of the Becke and Johnson process. It has quickly proven its efficiency compared to the most commonly used functional such as the GGA. In the FP-LAPW method, the wave function, charge density and potential are developed by spherical harmonic functions inside

the spheres around the atomic sites (muffin-tin spheres) and by a plane wave basis in the interstitial region of the unit cell. The maximum value of l for the development of the wave function inside the spheres was limited to $l_{\max} = 10$. The RMT plane wave cut-off factor $K_{\max} = 8$ was chosen for the development of the wave functions in the interstitial region while the charge density is grown in Fourier series to $G_{\max} = 14$ (Ryd)$^{1/2}$. RMT values were chosen equal to 1.86, 2.10 and 2.03 a.u for Mg, Y, and Ga atoms, respectively. The integration of k in the Brillouin zone is performed using the approach of Monkhorst and Pack [37], giving 47 k-special points in the Brillouin irreducible zone. The RMT parameter $K_{\max}$ and the number of special points have been varied to ensure the convergence of the total energy. The electronic configurations of the chemical elements which make up MgYGa compound are: Mg: [Ne] $3s^2$, Y: [Kr] $4d^1$ $5s^2$ and Ga: [Ar] $3d^{10}$ $4s^2$ $4p^1$.

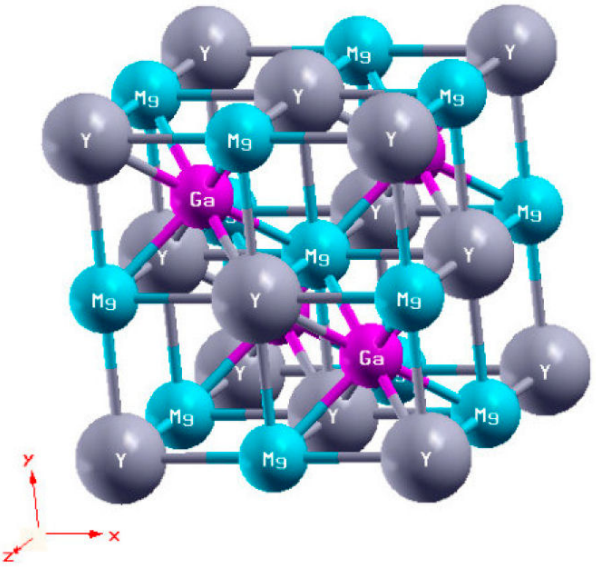

FIGURE 1. Schematic representation of the structure of MgYGa compound in α-phases.

3. Structural properties

The most important step in any ab-initio study is the determination of the structural properties of the compound. The knowledge of this information, allows us to calculate others physicals properties such as electronic and optical properties. MgYGa Half-Heusler alloy have a formula of XYZ where X is Mg, Y is Y and Z is Ga. We know well that in the zinc-blend structure, the anion takes the position T_1 (0,0,0) and the cation occupies T_2 (1/4,1/4,1/4) and the two interstitial sites T_3 (1/2,1/2,1/2) and T_4 (3/4,3/4,3/4) near the cation, are vacant. To obtain the Half Heusler compounds there are three possibilities to fill the sites: the anion always takes the position T_1(0,0,0) (in our case it is the Y atom). If the Z atom occupies T_2 and the X atom employs T_3, we get the α phase, and if occupies T_4 we get the β phase. The γ phase is obtained when the Z atom is in T_3 and the X atom is in T_2. But the Half-Heusler Materials are in most part stable in α phases. For this reason, we have calculated the structural properties of MgYGa compound in the α phase where the Mg, Y and Ga atoms occupy the positions (1/2,1/2,1/2), (0,0,0) and (1/4,1/4,1/4) respectively. For information, the α phases is just the zinc blend structure with F43m space (No. 216) groups. Figure 1 shows the representation of the conventional cell of MgYGa compound in α-phases. MgYGa compound has only three atoms in its primitive cell. The total energy of this compound was calculated as a function of volume, and we obtained a graphic of energy versus volume in Fig. 2.

This graph was fitted to the Murnaghan [38] equation of state [see Eq. (1)] in order to calculate the equilibrium lattice parameter, bulk module and the pressure derivative of the bulk module of the MgYGa compound.

$$E(V) = E_0 + \left(\frac{B_0 V}{B'(B'-1)}\right) \cdot \left(B'\left[1 - \frac{V_0}{V}\right] + \left[\frac{V_0}{V}\right]^{B'} - 1\right), \qquad (1)$$

where, B_0 and B' are bulk modulus and pressure derivative of the bulk modulus in the equilibrium volume V_0, respectively.

To prove the possible experimental simulation, a study of alloy is conducted to determine its energy formation. Energy formation of an atom is the fundamental difference between the mean energy of individual atoms without interaction and the energy of the crystalline structure. The energy of formation (E_{Form}) for the MgYGa compound is determined by the following expression:

$$E_{\text{Form}}(\text{MgYGa}) = E_{\text{Tot}}^{\text{MgYGa}} - E(\text{Mg}) - E(\text{Y}) - E(\text{Ga}), \qquad (2)$$

in which $E(\text{Mg})$, $E(\text{Y})$ and $E(\text{Ga})$ are the fundamental state energies per atom of Mg, Y and Ga, respectively. E_{Tot} (MgYGa) is the total energy of MgYGa compound.

The formation energy calculated for the compound MgYGa is -8.807 eV/atom (See Table I). This negative result shows that energy is acquired during the formation process, which reinforces the fact that the alloy is not only structurally stable but can also, be simulated experimentally. So, from the explanation above we can say that the alloy is thermodynamically stable.

The obtained results for the lattice parameter a_0, the energy of formation E_{Form}, the modulus of compressibility B and its derivative B' for the MgYGa compound are grouped

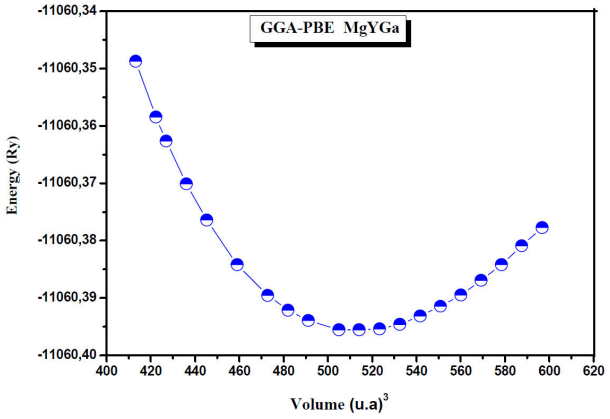

FIGURE 2. The total energies calculated MgYGa compound as a function of volume with the GGAPBE approximation.

TABLE I. Calculations of lattice parameter (a_0), bulk modulus B(GPa), pressure derivative (B'), volume V(Å)^3 and the energy of formation for MgYGa compound.

Compound	a_0 (Å)	B (GPa)	B'	E_0 (eV)	E_{form} (eV/atom)
MgYGa	4.817*	49.972	3.948	-150484.39	-8.807

*Present calculations.

in Table I. According to our knowledge, there are no experimental and theoretical data available to compare our results obtained.

4. Electronic properties

4.1. Band structure and density of states

In this section, we have, firstly, calculated and plotted the band structure of the MgYGa alloy by using the two approximations GGA-PBE and TB-mBJ for the calculation of band structure. Figure 3a) illustrates the band structure with GGA-PBE. We see, from this figure, that there is a small overlapping at the Fermi energy level between the maximum of the valance band (MVB) and the minimum of the conduction band (MCB). With TB-mBJ approximation [See Fig. 3b)], a slight shift of the MBV and MBC downwards and upwards, respectively, has been observed. In the two graphs, there is no gap, so, the compound has a metallic character. Also, the partial DOS is depicted in Fig. 4. From this figure, the dominant states in the energy range [-3, 0 eV], in the valence band, are the s-p Mg, p-Ga states, whereas d-Y states have a low contribution. In the energy range [0.2, 3 eV], the dominant states are mainly due to the d-Y states with the existence of a minority of the p-d Mg and p-Ga states.

5. Optical properties

In order to study optical properties of MgYGa compound, we calculated optical constants such as dielectric function, refractive index, extinction spectra, absorption spectra, and optical reflectivity. The optical parameters calculated are the response of the compound when electromagnetic radiation is introduced to them. The optical response of a material is given by its complex dielectric function $\varepsilon(\omega)$, which is defined by

$$\varepsilon(\omega) = \varepsilon_1(\omega) + \varepsilon_2(\omega). \tag{3}$$

The imaginary part, $\varepsilon_2(\omega)$, of the dielectric function $\varepsilon(\omega)$ is calculated from the momentum matrix elements of transi-

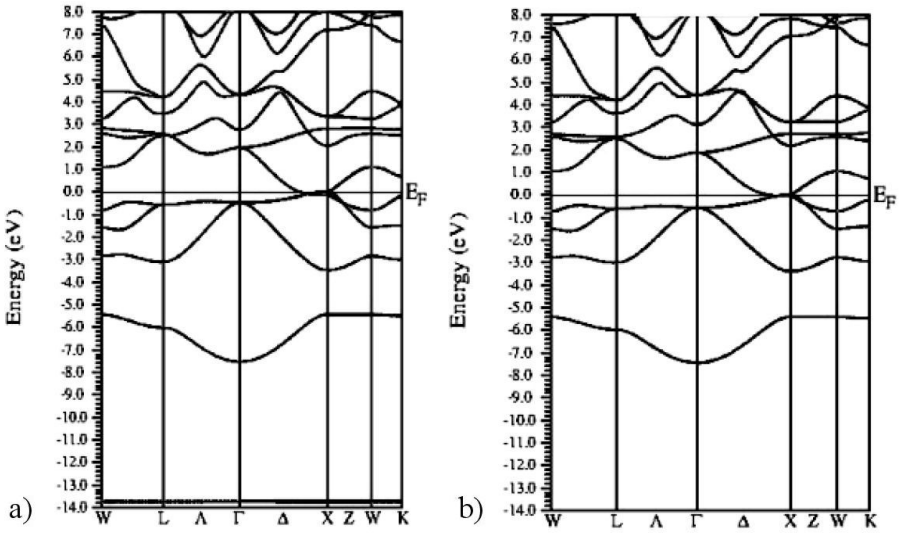

FIGURE 3. Calculated band structures of MgYGa compound obtained by: a) GGA-PBE and b) mBJ-GGA. The Fermi level is indicated by the horizontal line corresponding to zero energy (0 eV).

tion between the occupied and unoccupied electronic states and is given by

$$\varepsilon_2(\omega) = \frac{8}{3\pi\omega^2}\sum_{nn'}\int |P_{nn'}(k)|^2 \frac{dS_k}{\nabla\omega_{nn'}(k)}, \qquad (4)$$

where $P_{nn'}(k)$ are the elements of the dipole matrix between an initial state $nk\rangle$ and a final state $nk'\rangle$. Their self-energies are $E_n(k)$ and $E_{\dot{n}}(k)$ respectively, defining the quantity

$$\omega_{nn'}(k) = E_n(k) - E_{n'}(k). \qquad (5)$$

The real part of the dielectric function, $\varepsilon_1(\omega)$, is calculated from the imaginary part of the dielectric function using the Kramer-Kroening relation given by

$$\varepsilon_1(\omega) = 1 + \frac{2}{\pi}P\int_0^\infty \frac{\varepsilon_2(\omega')\omega'}{\omega'^2 - \omega^2}d\omega', \qquad (6)$$

where ω is the frequency, P is the main part of the Chauchy integral.

The refractive index $n(\omega)$ and the extinction coefficient $k(\omega)$ are given by [40].

$$n(\omega) = \frac{1}{\sqrt{2}}\left(\left[\varepsilon_1(\omega)^2 + \varepsilon_2(\omega)^2\right]^{1/2} + \varepsilon_1(\omega)\right)^{1/2}, \qquad (7)$$

$$k(\omega) = \frac{1}{\sqrt{2}}\left(\left[\varepsilon_1(\omega)^2 + \varepsilon_2(\omega)^2\right]^{1/2} - \varepsilon_1(\omega)\right)^{1/2}. \qquad (8)$$

5.1. Dielectric function

We have calculated and plotted the variations of the real and imaginary parts of the dielectric function, respectively, as a function of the frequency ω in Figs. 5 and 6, respectively. The real part of complex dielectric function ε_1 gives information about the physical properties of a compound and the imaginary part ε_2 is related with the electron transition

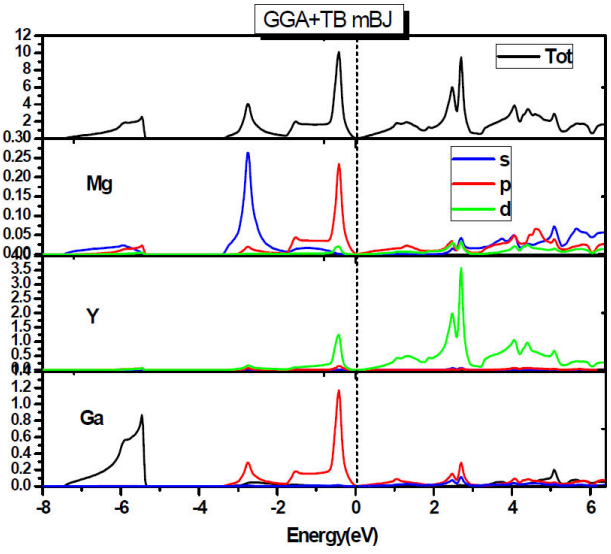

FIGURE 4. The partial and total electronic density of states graphs of the MgYGa compound.

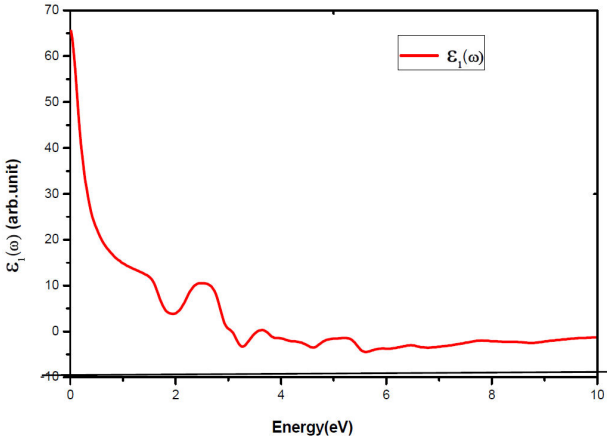

FIGURE 5. The real part, $\varepsilon_1(\omega)$ of the dielectric function of MgYGa compound.

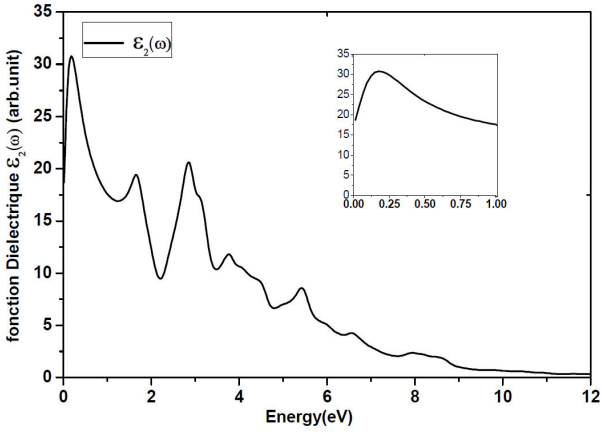

FIGURE 6. The imaginary part, $\varepsilon_2(\omega)$ of the dielectric function of MgYGa compound.

between the bands. From Fig. 5, the zero of real part of dielectric function ε_1, which corresponds to the location of the screened plasma frequency, is located at 3 and 3.6 eV. The negative values indicate the reflection of incident radiation from the surface. The value of ε_1 at zero photon energy is the static dielectric constant, which is equal to 65 for MgYGa compound. Figure 6 shows the imaginary part of the dielectric function, $\varepsilon_2(\omega)$ of the MgYGa alloy. The figure indicates that there are five peaks located at 0.2, 1.6, 2.8, 3.7, 5.4 eV in the energy range [0, 12 eV]. These peaks in the imaginary part indicate the transition electrons between the bands.

5.2. Refractive index and extinction coefficient

The refractive index $n(\omega)$ and extinction coefficient $k(\omega)$ are calculated using Eqs. (5) and (6), and are shown in Figs. 6 and 7, respectively. The refractive index is a very important physical parameter related to the microscopic interactions. The static refractive index $n(0)$

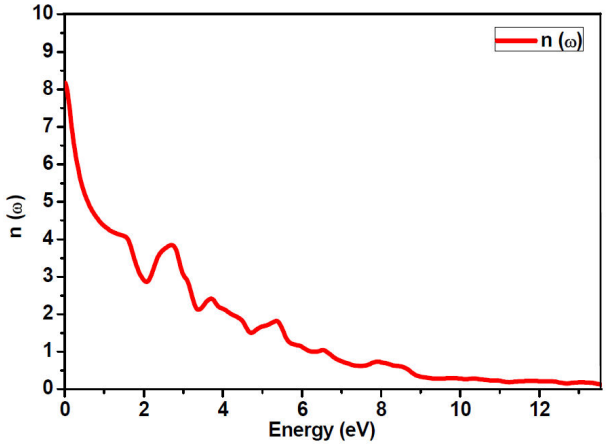

FIGURE 7. Refractive index of MgYGa compound.

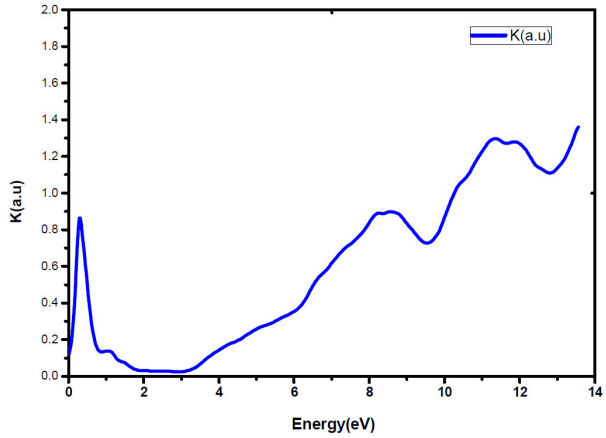

FIGURE 8. Extinction coefficient of MgYGa compound.

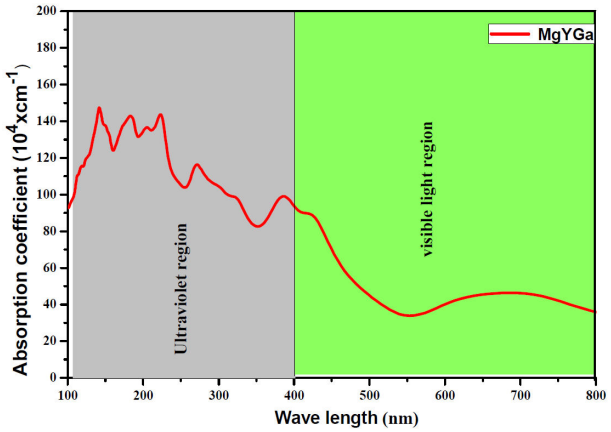

FIGURE 9. Absorption Coefficient of MgYGa compound.

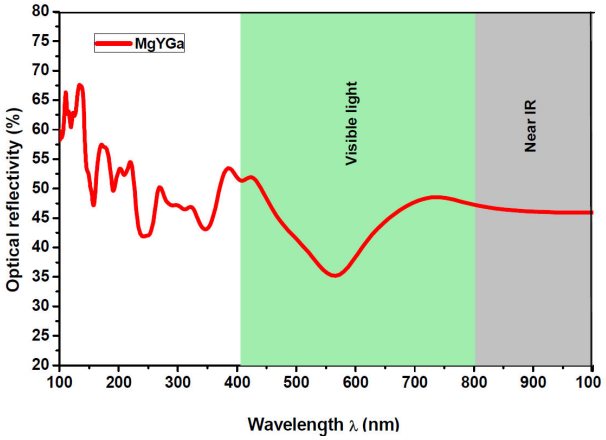

FIGURE 10. Optical reflectivity of MgYGa compound.

obtained is 8.2. We also note that the values of this parameter decrease when the photon energy increase. $k(\omega)$ provides a measure of absorption of incident radiation. From Fig. 8, the extinction coefficient $k(\omega)$ becomes very low in the energy range between [1, 3.2 eV] indicating very low absorption of light, which is favorable for transparent properties of the material in this range of the photon energy. On the other hand, it is clear from the figure that the alloy becomes light absorbent when the energy of the photon increases.

5.3. Absorption coefficient

The absorption coefficient defines how far light of a particular wavelength can penetrate into a material before being absorbed. If a material has a low absorption coefficient, light will be poorly absorbed, and a really thin material can appear transparent to that certain wavelength. Using the real and imaginary parts of dielectric function, the optical absorption coefficient is defined as

$$\alpha(\omega) = \frac{4\pi}{\lambda} k(\omega). \tag{9}$$

The variation of the absorption coefficient α with wavelength λ is represented in Fig. 9. We notice a decrease in light absorption when going from high energies (Uv light) to low energies (Vis light). In higher energies, the absorption is due to the transition between valance and conduction band. On the other hand, the contribution of absorption spectrum in low energies may be related to the transition between energy levels in a band.

5.4. Reflectivity

The reflectivity coefficient $R(w)$ is a measure of the amount of electromagnetic radiation reflected from the incident medium and is calculated using Eq. (10) [39]. The behavior of the reflectivity versus energy is plotted in Fig. 10.

$$R(\omega) = \left| \frac{\sqrt{\varepsilon(\omega)} - 1}{\sqrt{\varepsilon(\omega)} + 1} \right|^2 = \frac{(n-1)^2 + k^2}{(n+1)^2 + k^2}. \tag{10}$$

6. Conclusion

We have presented the structural, electronic and optical properties of half-Heusler MgYGa alloy using first principle methods. The structural parameters such as lattice parameter,

bulk modulus and its pressure derivative have been calculated for the first time. The negative energy of formation indicates that the compound is structurally stable. According to the electronic properties, the MgYGa presents a metallic character. We have also calculated the optical properties such as complex dielectric, refraction, absorption, extinction and reflection coefficients. We found that the optical properties of MgYGa vary according to the photon energies and can be beneficial to numerous applications.

1. H. Hohl *et al.*, Efficient dopants for ZrNiSn-based thermoelectric materials, *J. Phys. Condens. Matter* **11** (1999) 1697, https://doi.org/10.1088/0953-8984/11/7/004g.
2. G. Nolas, J. Poon, and M. Kanatzidis, Recent Developments in Bulk Thermoelectric Materials, *MRS Bull.* **31** (2006) 199, https://doi.org/10.1557/mrs2006.45g.
3. C. Yu *et al.*, High-performance half-Heusler thermoelectric materials $Hf_{1-x}Zr_xNiSn_{1-y}Sb_y$ prepared by levitation melting and spark plasma sintering, Acta Mater. **57** (2009) 2757, https://doi.org/10.1016/j.actamat.2009.02.026g.
4. I. Galanakis, Ph. Mavropoulos, and P. H. Dederichs, Electronic structure and SlaterPauling behaviour in half-metallic Heusler alloys calculated from first principles, *J. Phys. D: Appl. Phys.* **39** (2006) 765, https://doi.org/10.1088/0022-3727/39/5/S01g.
5. V. Dinh, K. Sato, and H. Yoshida, First Principle Study of Spinodal Decomposition Thermodynamics in Half-Heusler Alloy $CoTi_{1-x}$ Fe_x Sb, J. Su- percond. *Nov. Magn.* **23** (2010) 75, https://doi.org/10.1007/s10948-009-0573-7g.
6. L. Huang *et al*., Recent progress in half-Heusler thermoelectric materials, *Materials Research Bulletin* **76** (2016) 107, https://doi.org/10.1016/j.materresbull.2015.11.032g.
7. D. Kieven *et al*., I-II-V half-Heusler compounds for optoelectronics: Ab initio calculations, *Phys. Rev. B* **81** (2010) 075208, https://doi.org/10.1103/PhysRevB.81.075208g.
8. S. Yuasa *et al*., Giant tunneling magnetoresistance up to 410% at room temperature in fully epitaxial Co/MgO/Co magnetic tunnel junctions with bcc Co(001) electrodes, *Appl. Phys. Lett*. **89** (2006) 042505, https://doi.org/10.1063/1.2236268g.
9. S. S. P. Parkin *et al*., Giant magnetoresistance in magnetic nanostructures, *Annu. Rev. Mater. Sci*. **25** (1995) 357, https://doi.org/10.1146/annurev.ms.25.080195.002041g.
10. I. Zutic, J. Fabian, and S. Das Sarma, Spintronics: Fundamentals and applications, *Rev. Mod. Phys*. **76** (2004) 323, https://doi.org/10.1103/RevModPhys.76.323g.
11. B. Hülsen, M. Scheffler, and P. Kratzer, Thermodynamics of the Heusler alloy Co2-x Mn1+xSi: A combined density functional theory and cluster expansion study, *Phys. Rev. B* **79** (2009) 094407, https://doi.org/10.1103/PhysRevB.79.094407g.
12. T. Graf, C. Felser, and S. Parkin, Simple rules for the understanding of Heusler compounds, *Progress in Solid State Chemistry* **39** (2011) 1, https://doi.org/10.1016/j.progsolidstchem.2011.02.001g.
13. F. Benzoudji *et al*., Insight into the structural, elastic, electronic, thermoelectric, thermodynamic and optical properties of MRhSb (M=Ti, Zr, Hf) half- Heuslers from ab initio calculations, *Chin. J. Phys*. **59** (2019) 434, nurlfhttps://doi.org/10.1016/j.cjph.2019.04.009g.
14. S. Wolf *et al*., Spintronics: a spin-based electronics vision for the future, *Science* **294** (2001) 1488, https://doi.org/10.1126/science.1065389g.
15. T. Dietl *et al*., Zener model description of ferromagnetism in zinc-blende magnetic semiconductors, *Science* **287** (2000) 1019, https://doi.org/10.1126/science.287.5455.1019g.
16. J. Balluff *et al*., Integration of antiferromagnetic Heusler compound Ru2MnGe into spintronic devices, *Appl. Phys. Lett*. **111** (2017) 032406, https://doi.org/10.1063/1.4985179g.
17. S. Gupta and K. Suresh, Review on magnetic and related properties of RTX compounds, *Journal of Alloys and Compounds* **618** (2015) 562, https://doi.org/10.1016/j.jallcom.2014.08.079g.
18. T. Graf *et al*., Phase separation in the quaternary Heusler compound $CoTi_{1-x}Mn_xSb$-A reduction in the thermal conductivity for thermoelectric applications, *Scr. Mat.* **63** (2010) 1216, https://doi.org/10.1016/j.scriptamat.2010.08.039g.
19. S. Sakurada and N. Shutoh, Effect of Ti substitution on the thermoelectric properties of (Zr, Hf) NiSn half-Heusler compounds, *App. Phys. Lett*. **86** (2005) 082105, https://doi.org/10.1063/1.1868063g.
20. M. Katsnelson *et al*., Half-metallic ferromagnets: From band structure to many-body effects, *Rev. Mod. Phys.* **80** (2008) 315, https://doi.org/10.1103/RevModPhys.80.315g.
21. R. D. Groot *et al*., New class of materials: half-metallic ferromagnets, *Phys. Rev. Lett*. **50** (1983) 2024, https://doi.org/10.1103/PhysRevLett.50.2024g.
22. I. Galanakis Dederichs, and N. Papanikolaou, Slater-Pauling behavior and origin of the half-metallicity of the full-Heusler alloys, *Phys. Rev. B* **66** (2002) 174429, https://doi.org/10.1103/PhysRevB.66.174429g.
23. M. Singh *et al*., Effect of substituting sp-element on half metallic ferromagnetism in NiCrSi Heusler alloy, *Computational Materials Science* **53** (2012) 431, https://doi.org/10.1016/j.commatsci.2011.08.037g.

24. H. S. Saini *et al*., Generating magnetic response and halfmetallicity in GaP via dilute Ti-doping for spintronic applications, *Journal of Alloys and Compounds* **649** (2015) 184, https://doi.org/10.1016/j.jallcom.2015.06.278g.

25. P. Brown *et al*., The magnetization distributions in some Heusler alloys proposed as half-metallic ferromagnets, *Journal of Physics: Condensed Matter* **12** (2000) 1827, https://doi.org/10.1088/0953-8984/12/8/325g.

26. P. Brown *et al*., Atomic order and magnetization distribution in the half metallic and nearly half metallic C1b compounds NiMnSb and PdMnSb, *Journal of Physics: Condensed Matter* **22** (2010) 206004, https://doi.org/10.1088/0953-8984/22/20/206004g.

27. Y. Sakuraba *et al*., Huge spin-polarization of L21- ordered Co2MnSi epitaxial Heusler alloy film, *Japanese journal of applied physics* **44** (2005) L1100, https://doi.org/10.1143/JJAP.44.L1100g.

28. R. Shan *et al*., Demonstration of halfmetallicity in fermileveltuned Heusler alloy Co 2 FeAl 0.5 Si 0.5 at room temperature, *Phys. Rev. Lett.* **102** (2009) 246601, https://doi.org/10.1103/PhysRevLett.102.246601g.

29. Y. Fujita *et al*., Spin Transport and Relaxation up to 250 K in Heavily Doped n-Type Ge Detected Using Co 2 FeAl 0.5 Si 0.5 Electrodes, *Phys. Rev. App.* **8** (2017) 014007, https://doi.org/10.1103/PhysRevApplied.8.014007g.

30. P. Webster *et al*., Magnetic order and phase transformation in Ni2MnGa, *Philosophical Magazine B* **49** (1984) 295, https://doi.org/10.1080/13642817408246515g.

31. Please complete the information, (Ref. not found)

32. P. Hohenberg and W. Kohn, Inhomogeneous Electron Gas, *Physical Review* **136** (1964) B864, https://doi.org/10.1103/PhysRev.136.B864g.

33. J. P. Perdew, K. Burke, and M. Ernzerhof, Generalized Gradient Approximation Made Simple, *Phys. Rev. Lett.* **77** (1996) 3865, https://doi.org/10.1103/PhysRevLett.77.3865g.

34. F. Tran and P. Blaha, Accurate Band Gaps of Semiconductors and Insulators with a Semilocal Exchange-Correlation Potential, *Phys. Rev. Lett.* **102** (2009) 226401, https://doi.org/10.1103/PhysRevLett.102.226401g.

35. H. J. Monkhorst and J. Pack, Special points for Brillouin-zone integrations, *Phys. Rev. B* **13** (1976) 5188, https://doi.org/10.1103/PhysRevB.13.5188g.

36. F. D. Murnaghan, The compressibility of media under extreme pressures, *PNAS* **30** (1944) 244, https://doi.org/10.1073/pnas.30.9.244g.

37. P. Ravindran *et al*., Electronic structure, chemical bonding, and optical properties of ferroelectric and antiferroelectric NaNO2, *Phys. Rev. B* **59** (1999) 1776, https://doi.org/10.1103/PhysRevB.59.1776g.